Controlling the Optical Properties of Plasmonic Disordered Nanohole Silver Films

Thomas H. Reilly III,[†] Robert C. Tenent,[‡,§] Teresa M. Barnes,[†] Kathy L. Rowlen,[‡,⊥] and Jao van de Lagemaat[†,*]

[†]National Renewable Energy Laboratory, 1617 Cole Boulevard, Golden, Colorado 80401-3393 and [‡]Department of Chemistry and Biochemistry, University of Colorado, Boulder, 80309-0215. [§]Present address: National Renewable Energy Laboratory. [⊥]Present address: InDevR, Inc., 2100 Central Avenue, Suite 106, Boulder, Colorado 80301.

ABSTRACT Disordered nanohole arrays were formed in silver films by colloidal lithography techniques and characterized for their surface-plasmon activity. Careful control of the reagent concentration, deposition solution ionic strength, and assembly time allowed generation of a wide variety of nanohole densities. The fractional coverage of the nanospheres across the surface was varied from 0.05—0.36. Electrical sheet resistance measurements as a function of nanohole coverage fit well to percolation theory indicating that the electrical behavior of the films is determined by bulk silver characteristics. The transmission and reflection spectra were measured as a function of coverage and the results indicate that the optical behavior of the films is dominated by surface plasmon phenomena. Angle-resolved transmission and reflection spectra were measured, yielding insight into the nature of the excitations taking place on the metal films. The tunability of the colloidal lithography assembly method holds much promise as a means to generate customized transparent electrodes with high surface plasmon activity throughout the visible and NIR spectrum over large surface areas.

KEYWORDS: surface plasmon · transparent electrode · enhanced optical transmission · nanohole · nanoaperture · colloidal lithography · layer-by-layer deposition.

Surface plasmons (SP), collective electron oscillations at the surface of noble metals, have demonstrated tremendous potential as a route to tailor and selectively amplify myriad optical phenomena in molecular thin films.[1−11] A simple method for the integration of plasmon active materials into opto-electronic devices is the addition of metal nanoparticles.[10,12−17] An alternate route to introduce plasmon effects is the addition of subwavelength scale holes in a metal surface.[18−24] We have recently used this approach in an organic photovoltaic device.[25] Here we present a thorough characterization of the electrical and optical properties of random nanohole arrays as a function of hole density. Our aim is to evaluate the potential of these films as transparent conductors where both high transmissivity and low resistance play a critical role in overall performance.

The optical properties of nanometer-sized holes in metal films have been the focus of intense research.[19,23,26−36] The majority of the work has examined materials with regular periodic hole structures. The most significant finding concerning ordered nanohole films in silver has been the surprising magnitude of transmission reported. Such "enhanced optical transmission" has been explained as a surface plasmon assisted transmission process. The basic mechanism for the transmission process is (1) a photon couples to a SP on the incident side of a nanohole film, (2) the SP propagates within the hole to the opposite side of the film, (3) the SP is converted back to a photon and radiated into the far-field.[37] The energy of the photons resonant with the enhanced transmission process can be tuned by varying the metal in use, usually gold or silver, or by changing the characteristics of the ordered nanohole array. Characteristics such as the hole diameter, hole shape, hole spacing (lattice constant), film thickness, and array type (hexagonal, square, trigonal, *etc.*) can be used to tune the SP energy to specific wavelengths. The dielectric surroundings can also be used to manipulate SP resonances. The most widely used starting point to describe how SP resonances depend on a square nanohole array structure is the equation:

$$\lambda_{max}\sqrt{i^2 + j^2} \approx a_0\sqrt{\frac{\varepsilon_m\varepsilon_d}{\varepsilon_m + \varepsilon_d}} \qquad (1)$$

where λ_{max} is the normal incidence transmission maximum, i and j are indices identifying scattering modes from the periodic lattice, a_0 is the array lattice constant, ε_m is the real part of the dielectric constant of the metal, and ε_d is the real part of the dielectric constant of the surroundings. Even

*Address correspondence to jao.vandelagemaat@nrel.gov.

Received for review May 7, 2009 and accepted January 18, 2010.

Published online January 29, 2010.
10.1021/nn901734d

© 2010 American Chemical Society

though this simple equation omits many important factors, such as those mentioned above, it is highly effective in estimating the basic transmission behavior of a nanohole array.

Surface plasmons are additionally described according to their degree of localization. A localized surface plasmon (LSP) is typically used to describe the oscillation of electrons on a nanoparticle or around a nanohole. A propagating surface plasmon (PSP) is an excitation that is localized to a metal nanoparticle or nanohole and propagates on a flat film. These two subtly different renditions of surface plasmon excitations can interact and interconvert if the proper conditions are met. Numerous experimental studies exist that demonstrate the interconversion and constructive and destructive interference of LSPs and PSPs.[38−41] Studies involving LSPs and PSPs usually employ the use of near field scanning optical microscopy with dramatic modulation of the near field optical electric field distributions observed due to SPs. Recently it has also been verified that the interaction of LSPs and PSPs at close distances can modulate the far-field scattering of nanostructures. The interaction of LSPs with PSPs can be viewed as an additional mechanism to tune the optical behavior of nanostructured thin films and nanoparticle assemblies. Improved understanding of how this additional coupling mechanism influences far field optical properties may lead to greater application of plasmonic technologies.

While the majority of work on SP-enhanced transmission phenomena has focused on ordered nanohole arrays, facile methods to fabricate such arrays over large areas have remained limited thereby reducing widespread implementation. Simple nanolithography methods such as nanosphere lithography can be extended to create ordered hexagonal close packed arrays[42] but, it is often the case that the highly ordered regions of nanospheres form in unpredictable locations on the surface. While this may not impede fundamental optical characterization it does create additional challenges when the arrays are intended for studies in optoelectronic devices such as solar cells or light emitting diodes. In these studies one must be able to reproducibly locate the nanohole patterns in the same location on a substrate over a sufficiently large area such that multilayered architectures and macroscopic characterization can be accomplished. Therefore, a facile method that can reproducibly create a surface of nanoholes in an arbitrary metal film over large areas may enable research in plasmonics not currently achievable with the low throughput, small area, and/or unpredictable location of the most common nanolithography methods.

Additional advantages may exist in the use of metal nanohole films because of their high electrical conductivity. This allows the films to serve in a multiplexed sensing platform, for example, electrical and optical sensing, or as we have demonstrated to serve as an optical enhancing component in organic solar cells while also serving as a carrier extracting electrode. It is more difficult for SP active nanoparticle systems to perform dual optical and electrical roles since nanoparticles are isolated and means of electrically connecting them is nontrivial.

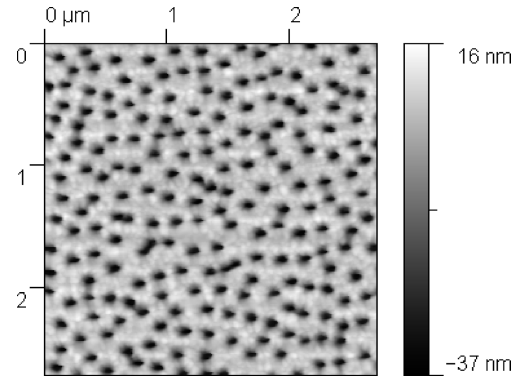

Figure 1. A representative atomic force micrograph of the disordered nanohole system studied.

A solution to the aforementioned application demands is the recent method published by Hanarp *et al*,[43] dubbed colloidal lithography; the method modifies an arbitrary surface with polyelectrolytes to carry a preferential charge such that oppositely charged commercially available latex spheres will bind to the surface owing to Coulombic attraction. Since the latex spheres are of like surface charge, they repel each other and avoid clustering on the surface. The Coulombic repulsion also prevents multilayers from forming on the surface ensuring a uniform nanosphere mask. A drawback of the technique presently is that the resulting nanosphere mask lacks long-range order. Short-range order does arise from the surface striving to find an electrostatic potential energy minimum so the nanoparticles do have a systematic mean separation distance.

The colloidal lithography method has been used to prepare random nanohole arrays to study the optical properties of single, isolated holes in a gold film.[44,45] Despite the ease with which random nanohole structures can be produced using simple and inexpensive processes, there have been relatively few publications that deal with their optical characterization and none that deal with electrical characterization. By understanding how to control the SP behavior of random nanohole films and how nanostructuring influences the electrical properties of the films, the widespread implementation of nanohole films in many applied fields of science becomes possible. Figure 1 shows a representative atomic force micrograph of the disordered nanohole film investigated in this study.

In this paper, we have thoroughly characterized the SP activity and electrical characteristics of silver nanohole films with a mean nanohole diameter of 92 nm and a constant silver film thickness of 40 nm. First, to achieve wide control over the nanosphere colloidal li-

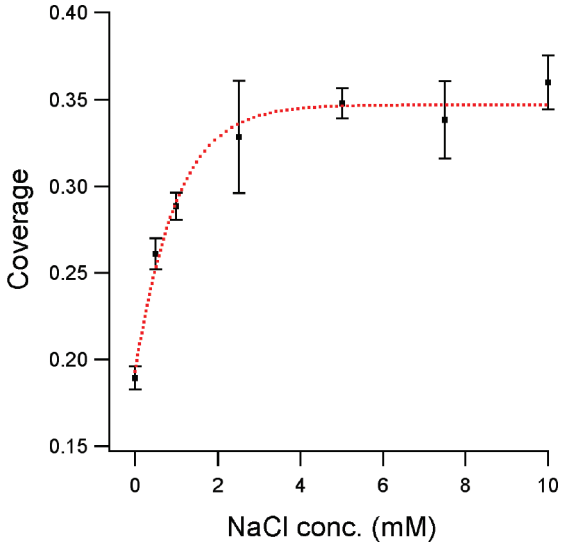

Figure 2. Nanohole coverage as a function of salt concentration in deposition solution. A sigmoidal fit has been added to guide the eye.

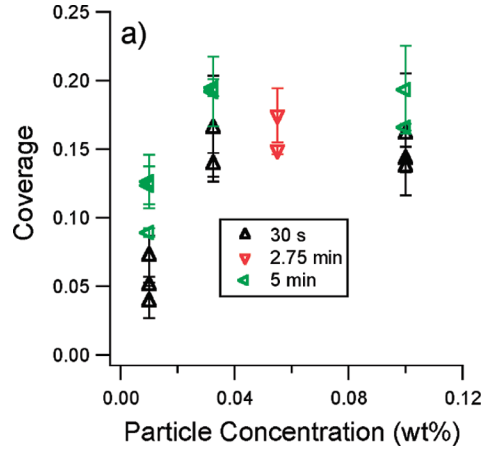

Figure 3. Plot of nanohole coverage as a function of particle concentration (wt %). The legend indicates the deposition time used for that sample set. The only way to achieve a coverage below 0.10 from this study was to use both a short deposition time and low solution concentration.

thography mask coverage and to obtain a greater understanding of the deposition process, deposition conditions such as nanosphere solution concentration, deposition time, and salt concentration were explored in greater detail than present in the literature. The observed optical effects can be interpreted as largely due to disordered grating structures and the electrical behavior follows closely to a simple percolation model. The plasmon behavior is compared to the body of literature surrounding this promising nanostructured system.

RESULTS AND DISCUSSION

Colloidal Lithography. Figure 1 shows an atomic force micrograph of a typical random nanohole film prepared using colloidal lithography. From AFM images, the fractional hole coverage and average hole-to-hole distance were determined. The colloidal lithography technique relies on repulsion between similarly charged latex spheres to provide spacing and eventual short-range order between the spheres when adsorbed on a charged surface. Using this technique, we found a maximum fractional coverage of 0.20 $\pm$ 0.03 (n = 11) for systems with no intentionally added salt. To obtain coverages higher than this we used the procedure outlined by Hanarp *et al.*[43] The hole density was adjusted by controlling the ionic strength of the deposition solution. As the salt concentration increases, more of the charge on the latex sphere becomes shielded thus allowing for control of the distance between spheres.

Figure 2 shows the fractional coverage of 92 nm holes in a 2.5 μm by 2.5 μm region of the surface as a function of NaCl concentration in the deposition solution. All depositions were performed with a 0.1% particle concentration and using a 30 min deposition time. The nanohole coverage increases rapidly upon the addition of salt and quickly approaches a limit at $\sim$ 0.35. Each data point represents an average for at least three 2.5 μm by 2.5 μm regions of a 1 in. by 1 in. surface.

For high-density samples, heat treatment by immersion in boiling, ultrapure water of the sample after the initial sphere deposition was found to be crucial to reduce multisphere aggregate formation. For high particle densities, the films are initially highly aggregated but upon heating the particles redistribute. The temperature of the hot bath was found to be crucial. It is important that the bath be at a boil prior to exposing deposited spheres. With the bath at lower temperatures, high-density samples were severely aggregated.

Surface coverages below 0.20 were obtained by adjusting both the solution particle concentration and the deposition time. Figure 3 shows the fractional surface coverage as a function of particle concentration. The highest particle concentrations and times used gave a surface coverage similar to those observed for the control experiments at 0.1% particle concentration and 30 min deposition times. As evidenced from the data, times in excess of five minutes are unlikely to have an appreciable effect on surface coverage. The measured surface coverages for all concentrations used with the exception of the 0.01% particle solution are statistically identical. This implies that particle concentration is the more significant factor in determining final surface coverage. We can also infer that while time does appear to have an effect on surface coverage, for the times examined (30 s to 5 min) the effect is small. No attempt was made to examine times shorter than 30 s. This was deemed impractical based on our current procedure. The data at the lowest particle concentration give the only statistically significant difference in surface coverage with a minimum coverage observed at 0.01% particle concentration and a deposition time of 30 s of 0.04 $\pm$ 0.01.

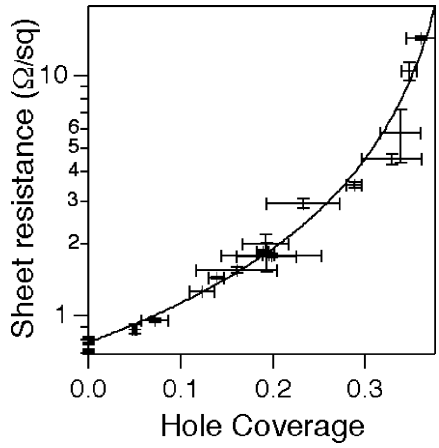

Figure 4. Sheet resistance of the nanohole films as a function of fractional hole coverage. The dotted line represents a fit to standard percolation theory indicating the electrical properties of the silver films are well described by bulk properties and geometric analysis.

The data taken as a whole show that while deposition time does play a factor in final surface coverage, in practice particle concentration determines the ultimate hole density. Close to maximum film density is achieved in under 30 s. The most practical way to control surface coverage is therefore by using low concentrations of particles with deposition times of no longer than 5 min.

Electrical Characterization. The sheet resistance of the films as a function of nanohole surface coverage is shown in Figure 4. For all cases measured, the sheet resistance was better than that typically reported for indium tin oxide coated glass substrates (*ca.* 15−30 Ω/sq). The influence of nanohole coverage on sheet resistance followed the well-known equation derived from percolation theory:

$$f(c) = A(c_{crit} - c)^{\eta} \qquad (2)$$

where A is a pre-exponential factor, c_{crit} is the critical nanohole coverage condition where the probability of a conducting pathway in the film falls to zero, c is the hole coverage, and η is the 2D conductivity exponent. Fitting the conductivity data to the percolation threshold equation yielded a c_{crit} value of 0.42 ± 0.01 and a 2D conductivity exponent of 1.37 ± 0.06. These results are identical to the percolation threshold values predicted and reported by others on similar systems that used much larger not nanosized holes.[46,47] This result indicates that while nanostructuring the surface can have strong nonclassical optical effects, the conductivity of the silver films as a function of hole coverage still follow a simple percolation threshold theory. This is of course not unexpected as the presence of the holes should only significantly impact the conduction mechanism in the silver film when the feature size drops below the electron mean free path, which is about 57 nm at room temperature.[48] The nanohole coverage in theory should be able to go to the limit of a hexagonal close packed arrangement but without access to precise ordering there is little advantage obtaining disordered hole coverages above a value of ~0.4 since it will result in a nonconductive film. The sheet resistance values observed here suggests these films have promising high current applications where the resistive losses of typical transparent conductors may result in poor performance.

Optical Characterization. Figure 5 shows transmission and reflection spectra taken for a series of nanohole films of different coverages. The transmission and reflection spectra were collected using an integrating sphere whereby both forward scattered and backscattered light are detected. The nanohole films show an increase in transmission magnitude and a decrease in reflection as coverage increases. When employing these films as transparent conductors one needs to strive for the highest nanohole coverage possible while still retaining a conductive film as the overall transmission of the films continues to rise with nanohole coverage. At specific wavelengths there are specific nanohole coverages that yield a maximum transmission, for example, ~550 nm, where increasing nanohole coverage does not increase transmission.

In square nanohole arrays, the transmission maxima of the array should depend linearly on the lattice constant. The random films do not have any long-range order but with increasing coverage, there is a systematic reduction in the average interparticle spacing. As an initial approximation the changes in coverage, and therefore hole-to-hole separation, observed for this disordered system may be thought of as a change in the lattice constant of the nanoholes. Equation 1 suggests one should observe a blue shift in the SP transmission maxima as the coverage increases and the hole-to-hole separation decreases. As can be seen in Figure 6, the transmission maxima are not strongly influenced by changes in hole-to-hole separation, estimated from the nanohole coverage. Figure 6 indicates that the different optical data collected contain unique information about the system under investigation. In contrast with the study of scattering and extinction from nanoholes in a thin gold film,[44] we do not observe a close linear relationship with hole-to-hole separation in transmission. By comparing the slope of the reflection data and transmission data, the reflection minima change more rapidly with hole-to-hole spacing than the transmission maxima. This is likely due largely to the difference in dielectric values between glass and air. Since the hole-to-hole separation is the same for transmission and reflection at each coverage, the ratio of the slope in transmission maxima and reflection minima should yield the ratio of the terms contained in the square route argument of eq 1. Using the real dielectric values of silver, glass and air at 550 nm predicts a slope of ~1.5. In this work, the ratio experimentally obtained is 6.3. Solving for the effective real dielectric value of sil-

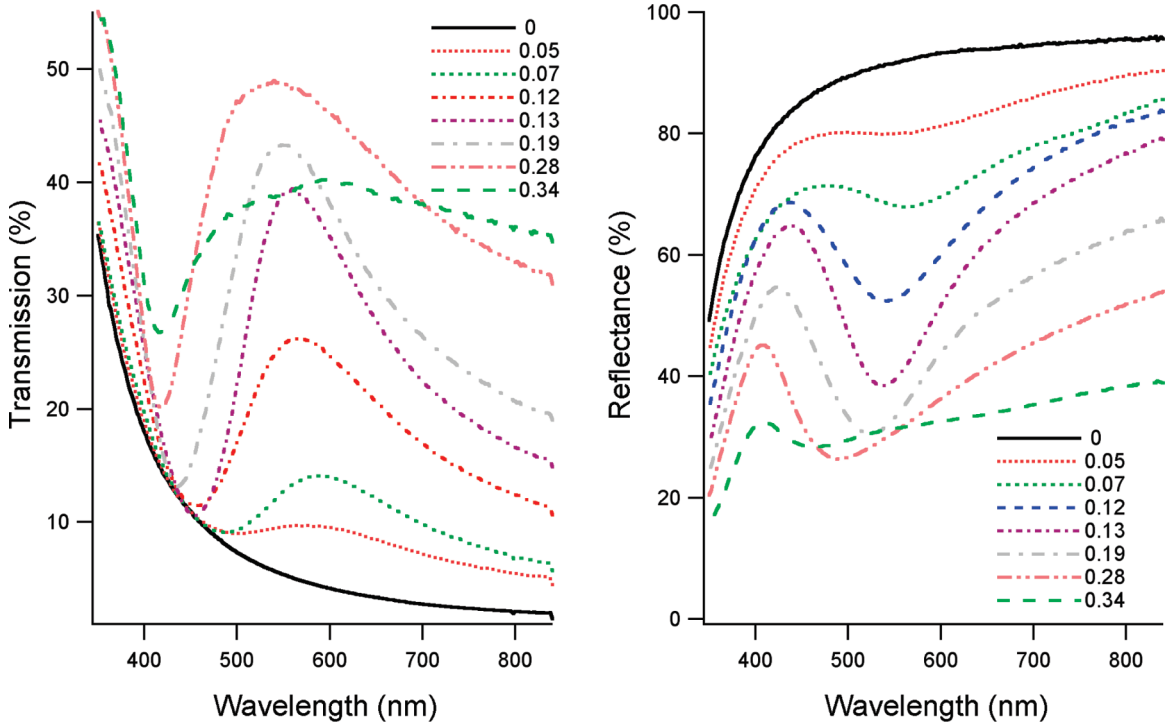

Figure 5. Transmission spectra (left) and reflectance spectra (right) measured with an integrating sphere for a series of nanohole silver films with varying nanohole coverage. The spectra demonstrate that the magnitude of transmission or reflectance can be tuned *via* nanohole coverage without changing the nanohole size. The inset legend indicates the nanohole coverage for each spectrum.

ver to support a slope ratio of 6.3 yields a value of −2. This value is far outside the accepted range of the optical constants of silver leading to the conclusion that the changes in the optical data must explained by phenomena beyond those contained in eq 1.

One explanation may be that the hole-to-hole separation is too small to compare with the work of Prikulus *et al* who studied hole-to-hole separations of 575 to 625 nm. The largest hole-to-hole separation studied in this work is estimated at 376 nm so the resulting first order grating coupling effects expected to arise from the nearest-neighbor nanohole separation distance are at

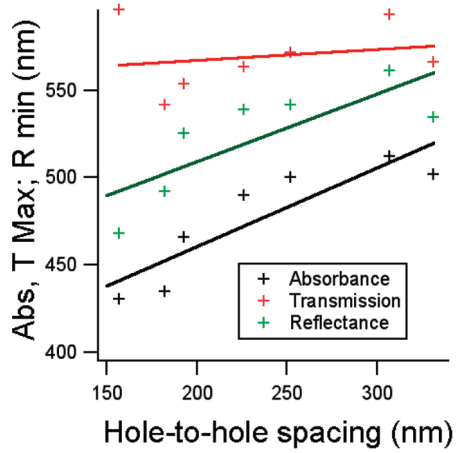

Figure 6. The measured transmission, absorbance maxima, and reflection minima *vs* the hole-to-hole separation for the disordered nanohole films. Linear fits to the maxima and minima have been added to guide the eye.

wavelengths below those investigated in this study. The nanohole films investigated here are effectively nondiffracting due to the short hole-to-hole separation.

A recent report on ordered, nondiffracting nanohole films in a square lattice with constants of 200, 225, and 250 nm (similar hole-to-hole separations as the present study) revealed that the transmission spectra can still be tuned somewhat by changing hole-to-hole separation even when lattice constants would suggest the nanoholes should be nondiffracting at visible wavelengths.[49] At these separation distances it has been proposed that the continuous film allows for the localized hole plasmon to couple *via* the PSP of the film to other localized hole plasmons. In this work we observe qualitatively the same effect, as the hole-to-hole separation decreases, the transmission peak moves to shorter wavelengths even though the hole-to-hole separation is much smaller than an effective lattice constant for visible wavelengths. This indicates that a similar nanohole coupling mechanism as discussed above for square lattices operates in the random nanohole arrays.

Enhanced optical transmission initially reported by Ebbesen and co-workers was defined as the transmitted power incident on the area of a subwavelength hole in an optically thick metal film. When the transmitted power through the hole exceeds that predicted by Bethe theory the transmission is "enhanced." Hanarp *et al* estimated based on individual extinction and dark field scattering measurements that the nanohole films in thin gold films exhibited an enhancement factor of ~5,

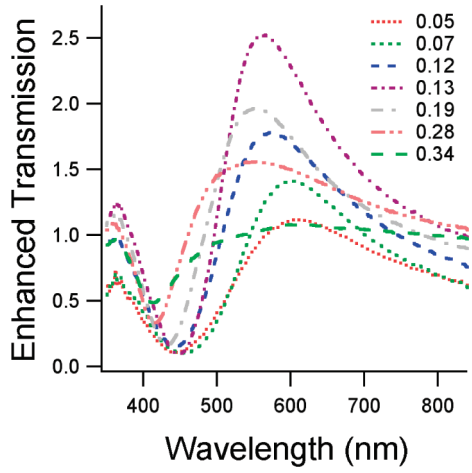

Figure 7. Enhanced optical transmission spectra calculated from the nanohole transmission spectra, nanohole coverage, and silver reference film spectrum. A value of 1 indicates no enhancement in transmission compared to the silver reference film, values greater than 1 indicate wavelengths that are enhanced. Values less than 1 indicate the films transmit less light than the silver reference film.

that is, at maximum transmission the holes transmitted five times more light than incident upon their geometric area. The results presented in this paper agree strongly with this estimation. The enhanced transmission spectra for the films in this work are shown in Figure 7. The spectra were calculated by subtracting the silver film reference spectra, weighted by the fraction of the area occupied by the silver film, and dividing by the fractional coverage occupied by the nanoholes. The magnitude of enhanced transmission reaches a maximum value of 2.5, in agreement with similar work on nanoholes in thin gold films.

The enhanced transmission maxima from Figure 7 are plotted as a function of hole-to-hole separation in Figure 8. The hole-to-hole separation was calculated using a two-dimensional radial distribution function derived from simulated nanohole distributions governed by Coulombic repulsion. (See Supporting Information for more information on the nanohole distributions.) While the hole-to-hole separation studies in this work

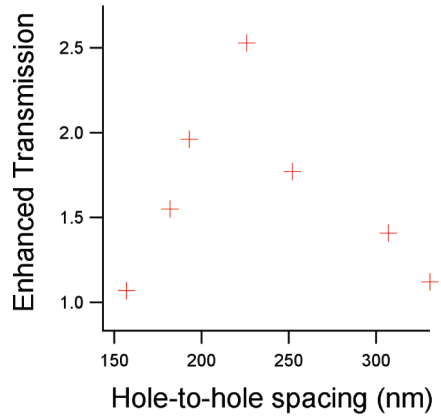

Figure 8. Enhanced transmission maxima for the nanohole coverages plotted *vs* hole-to-hole separation.

are over a short-range, it is easily seen that the nanoholes have a clear enhanced transmission resonance where the enhanced transmission rises well above a value of 1 but at the high and low coverages the enhanced transmission values remain close to 1. The observation that enhanced transmission does not continue to rise with nanohole density but appears to have a resonant coverage agrees with the recent work of Alaverdyan *et al*,[27] who modeled the interaction of 1-dimensional chains of nanoholes in thin gold films and experimentally measured the elastic scattering spectra of nanohole chains in thin gold films. It was observed that elastic forward scattering can be enhanced significantly when the amplitude of dipolar charge oscillations occurring at two closely spaced nanoholes is constructively combined with the charge oscillations of the antisymmetric bound PSP of the gold film. The constructive resonance condition is met when the edge to edge distance of the nanoholes is equal to $(n + 1/2)\lambda_{PSP}$, where $n = 0, 1, 2, ...$, and λ_{PSP} is the wavelength of the antisymmetric bound mode of the thin metal film. In the instance of thin films where the SPs at both interfaces can strongly couple with one another, the wavelength of the bound modes is roughly half the wavelength of the photon in free space.[27] With such small values of λ_{PSP}, the impact of LSP−PSP coupling can only be observed at small nanohole separations such as the ones studied in our case. The resonance effect can be observed in Figure 8 where at hole-to-hole separations of approximately 225 nm, the enhanced transmission spectra reach a maximum. Assuming this is the $n = 0$ case we estimate λ_{PSP} of a 40 nm silver film to be 266 nm (225 nm hole-to-hole separation = 133 nm edge-to-edge separation for 92 nm diameter nanoholes) for the antisymmetric bound PSP mode.

The absorbance of the nanohole films is shown in Figure 9. Since an integrating sphere was used to capture forward and backscattered light in the transmission and reflection data, the absorbance spectra do not contain a scattering component and they represent the real energy absorbed in the film. This is in contrast to extinction spectra typically reported in plasmonics literature that do not distinguish between scattered and absorbed photons. Perhaps the most striking element of the absorbance data is the observation of the dramatically rising long wavelength component of the absorbance spectrum at increasing coverages. Such a broad spectral plasmon response has been proposed to be integral to the application of SPs for solar energy harvesting.[50] AFM images revealed that as coverages approach the percolation threshold, an increased population of merged nanohole dimers and trimers is observed. Since nanohole transmission, and therefore film absorbance, red shift with increasing nanohole diameter, the merged nanoholes provide a distribution of effective nanohole diameters which may be responsible for the mainly featureless longer wavelength absor-

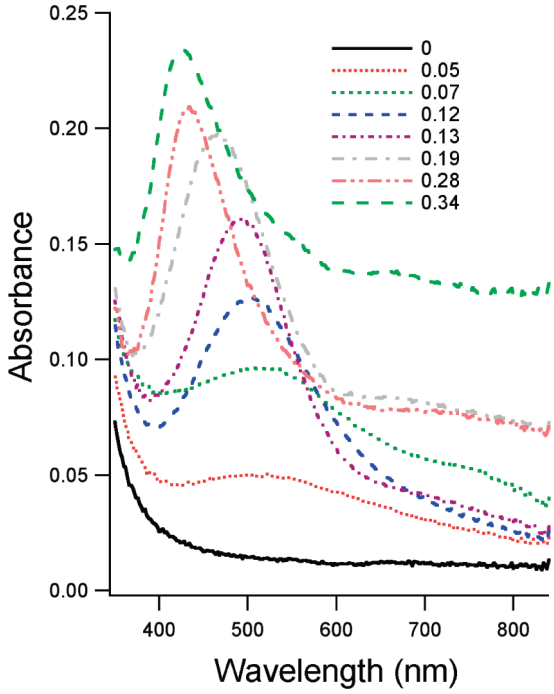

Figure 9. Absorbance spectra of the nanohole films as a function of nanohole coverage. With increasing nanohole coverage the films are capable of trapping more light at the surface. The absorbance maximum blue shifts as coverage increases and the integrated absorbance also increases across the wavelengths monitored.

bance observed beyond 600 nm at the highest coverages studied.

In analogy to the ordered nanohole arrays and isolated nanoholes, it is expected that the random nanohole array would exhibit angle dependent transmission and reflection spectra. Figure 10 shows polarization-resolved, angle-dependent extinction spectra of a nanohole film. Extinction was calculated from direct transmission and reflection measurements. As the angle of incidence increases, the extinction of p-polarized light shifts to higher energies. The main extinction feature appears to be composed of two closely overlapping peaks and the relative intensity of the high-energy peak to the low-energy peak increases as a function of angle of excitation. The s-polarized extinction spectra flatten and red shift slightly but are largely invariant compared to the p-polarized spectra. As the excitation angle increases, the electric field vector of the p-polarized light moves toward a perpendicular excitation of the film instead of a horizontal excitation. In s-polarized mode, the electric field vector is in the plane of the film and does not change with excitation angle. A perpendicular excitation should be constrained by the film thickness and the dimensions of the nanohole. Given these two criteria, it is reasonable to expect that the high-energy peak in the extinction spectra is a result of the nanohole cavity LSP mode whose oscillation is perpendicular to the substrate. The symmetry of this excitation is similar to the symmetric leaky mode of a continuous thin film, although it is not possible to directly excite this symmetry excitation in a flat thin film.[26]

The integrating sphere transmission and reflection measurements allow one to calculate the energy loss due to absorption. The energy-integrated absorbance data as a function of coverage has a positive slope for the coverages investigated in this work. Intuitively this extrapolation must not be correct, in the limit of very high nanohole coverage our data must converge with the dispersed nanoparticle data in the literature that indicates very low coverage nanometric silver particles will have low absorbance. This leads to the conclusion that the absorbance as a function of coverage must not fit linearly to coverage, it must ultimately return to zero absorbance at a nanohole coverage of 1 (zero silver content). This requirement indicates that the absorbance plot as a function of coverage should lead to a maximum that indicates how to best couple visible light to silver films. A simple polynomial fit to energy-integrated absorbance data (not shown) estimates a maximum absorbance at a coverage of 0.5 for this system. This may be useful for photothermal, photochemi-

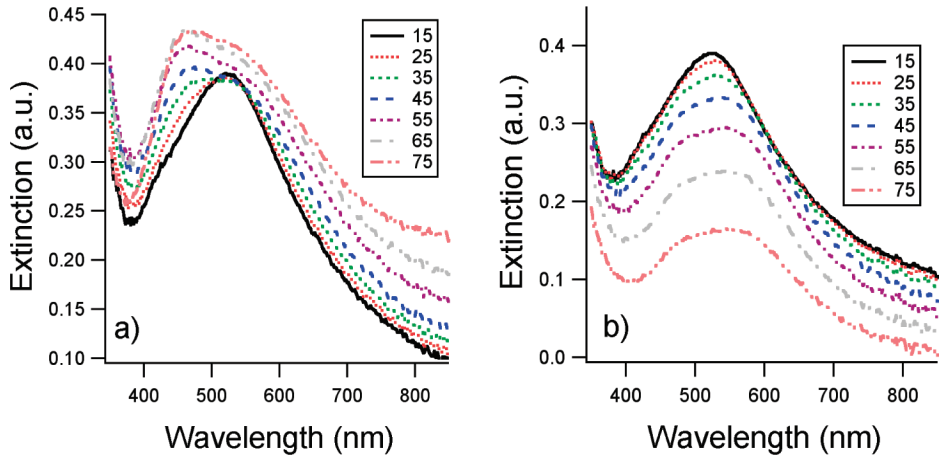

Figure 10. Extinction spectra of a nanohole film based on direct transmission and reflection measurements. The legends indicate the angle between excitation and collection optics for the film: (a) p-polarized extinction spectra of a nanohole film; (b) s-polarized extinction spectra from the same film.

cal, or photoelectrical applications where the mechanism for energy harvesting initiates by coupling photons to SPs in silver. For applications that require the silver films to remain conductive over long ranges, the maximum photon harvesting coverage has already been determined from the electrode data presented here to be ~0.4.

In summary, an extensive study of the electrical and optical properties of nanohole silver films was conducted. A detailed exploration of deposition conditions revealed that in order to achieve the lowest coverages, the latex sphere concentration must be reduced from previous reports and deposition times must be minimized. The nanohole films remain electrically conductive over the entire range of coverages studied. The electrical behavior is well described by a percolation model suggesting that the films can serve as effective conductive transparent electrodes up to coverages of 0.4. To obtain nanohole coverages higher than 0.4 it will be necessary to use ordered systems such as a hexagonal close packed nanohole arrays in order to retain conductive pathways. The optical properties of the nanohole films have been interpreted in light of their SP enhanced optical transmission properties. We observe close agreement with recent work describing ordered nondiffracting square nanohole arrays and random nanohole films in gold that indicate that at these coverages the far-field optical properties are strongly influenced by LSP−PSP coupling. Since the highest transparency nanohole films were achieved at the highest nanohole coverages with hole-to-hole separations below visible diffraction wavelengths, a deeper understanding of how LSP−PSP coupling influences a film's optical behavior is needed in order to take full advantage of plasmon enhanced transmission. With improved understanding, this multifunctional plasmonic system may see greater widespread implementation.

METHODS

Materials. The method of Hanarp *et al*[43] was initially followed to guide the further development of the colloidal lithography process. Sulfate modified latex spheres (92 nm diameter) in water (8% w/v) were purchased from Invitrogen Corporation, Carlsbad, CA. Poly(diallyldimethyl ammonium chloride (PDDA) (medium molecular weight) 20% in water and poly(sodium 4-styrene sulfonate) (PSS) 30 wt % solution in water were purchased from Aldrich Chemical Co., St. Louis, MO. Aluminum chlorohydrate was purchased from Spectrum Chemical Manufacturing Corporation, Gardena, CA. Sodium chloride Baker Analyzed Reagent grade was purchased from J.T. Baker Chemical Company, Phillipsburg, NJ. All chemicals were used as received without any further purification.

Solution Preparation. All solutions were made using 18.2 MΩ deionized water. All salt-containing solutions were prepared from dilutions of the same stock solution and were brought to the desired concentration prior to the addition of spheres.

Glass Substrate Cleaning. All samples were prepared on glass microscope slides. Slides were scrubbed using a sponge with a dilute solution of Liquinox following by rinses in tap water, house deionized water and a final rinse with 18.2 MΩ deionized water. The slides were blown dry using nitrogen. Following the water-based cleaning, slides were treated in an oxygen plasma (700 mTorr O_2, 150 W, 5 min process time). All depositions were performed within a few hours of, if not immediately following, the sample cleaning steps. Prior to exposure to the oxygen plasma, the glass slides were cut into roughly 1″ by 1″ squares. Samples were blown off with a nitrogen gun to remove any glass shards remaining from the scribing and breaking process.

Polyelectrolyte Glass Treatment. The glass surface was modified with a polyelectrolyte multilayer as demonstrated by Hanarp *et al*.[43] Slides were exposed to 30 s dips in 2% by weight solution of PDDA, 2% PSS, and 5% AlCH solutions sequentially. Samples were rinsed in a 18.2 MΩ water bath and blown dry with nitrogen following each exposure.

Controlled Sphere Deposition. A 0.5 mL aliquot of latex sphere solution was deposited on top of each 1″ × 1″ square of triple-layer treated glass slides. Samples were left in a closed Petri dish to avoid contamination and avoid solvent loss due to evaporation.

Dense packing of latex spheres was achieved by adding various concentrations of NaCl to the deposition solutions thereby reducing charge repulsion between spheres. All high coverage samples were deposited for 30 min.

Low coverage samples were generated in the absence of intentionally added salts and were controlled by varying both sphere concentration and deposition time

Post-Deposition Processing. Following the sphere deposition step, samples were rinsed with 18.2 MΩ deionized water. Maintaining the water meniscus over the top of the sample was found to be extremely crucial to obtaining bulk sample uniformity. Samples were maintained level during the rinsing step and rinsewater was added with a spray bottle. A gentle stream from the spray bottle was directed away from the center of the sample and to an area that was deemed noncritical to sample success. It was found that a direct sharp stream from the spray bottle could easily remove spheres from the sample surface. Water was streamed over the top of the sample until the meniscus was clear and appeared void of latex spheres. An alternate method to the gentle rinsing step using a spray bottle is to immerse the entire sample in a beaker of water to remove the excess spheres. For 1″ × 1″ glass substrates approximately 400 mL of 18.2 MΩ water was used as the rinse bath at room temperature. Provided a water meniscus remains over the surface of the sample through the entire process, this was determined to be an equally effective means of rinsing the excess sphere suspension. While still carefully maintaining a level surface to keep the meniscus intact, the rinsed sample was immersed in a beaker of boiling water for 60 s. The temperature of the heated bath was also found to be critical in suppressing large-scale aggregation of the spheres on the sample surface. When treated in a hot bath that was at a rolling boil, no large-scale aggregation was observed. If the hot bath was not at a rolling boil significant aggregation was observed. After the hot bath soak, samples were transferred, again with great care to maintain a water overcoating on the sample surface, into a cold bath. The exact temperature of the cold bath was not determined and certainly varied significantly during the preparation of large numbers of samples. Initially the cold bath was cooled to the point of containing several ice crystals. No attempt was made to control the temperature of the cold bath and the variability described did not appear to have any significant effect on sphere deposition results. After exposure to the cold bath, samples were transferred, again with careful attention to maintaining the sample level, onto a dry clean kimwipe, which allowed a significant volume of water to wick away. The sample was blown dry with nitrogen. A gentle stream of nitrogen was at first focused on the center of the sample allowing this region to dry first. The flow rate of the nitrogen stream was gradually increased to push the water "front" out toward the extreme edges of the sample surface. This was done

to keep any portion of the dried surface from rewetting. Rewetting of the already dried surface lead to large-scale surface nonuniformity in all cases.

Silver Film Deposition. Following the sphere deposition steps, silver was deposited at a rate of 1 Å/s starting with a base pressure of 1×10^{-7} Torr in a thermal evaporator (Ångstrom Engineering). In this study, the silver film thickness was kept constant at 40 nm.

Sphere Removal. Following silver deposition, the silver films with embedded spheres were sonicated in isopropyl alcohol. Samples were sonicated for several different times over the course of our experiments. Samples appeared to be stable with up to 15 min of sonication exposure. Shorter times often lead to incomplete removal of spheres. Several samples appeared to have spheres remaining after 30 min of sonication but this was unusual and these samples were excluded from the statistical nanohole analysis.

Optical Data Collection. Transmission and reflection data were collected using a Cary (2500) spectrophotometer with an integrating sphere attachment. A packed Teflon powder reflectance standard from LabSphere was used as a reference. The instrument baseline was established with the transmission holder empty and the reflectance standard in the reflectance holder.

AFM Analysis. Fractional nanohole coverage was calculated by counting the number of holes in the image, multiplying by the nominal area of a 92 nm diameter circle, and dividing by the total image area. Comparison was made to more complex software package systems for analysis, but for 92 nm structures tip artifacts were found to lead to significant error in measuring an accurate hole coverage.

Acknowledgment. T.H.R., J.v.d.L. and T.M.B. would like to acknowledge support from the Laboratory Directed Research and Development program at NREL. R.C.T. and K.L.R. would like to acknowledge support from the NSF. This work was supported by the U.S. Department of Energy under Contract No. DE-AC36-99GO10337 with the National Renewable Energy Laboratory.

Supporting Information Available: A description of the equations used for the calculation in this paper as well as an example of the calculated radial distribution function for a nanohole film. This material is available free of charge *via* the Internet at http://pubs.acs.org.

REFERENCES AND NOTES

1. Yamagishi, K.; Inoue, J.; Yamashita, M. Surface Plasmon Resonance in Organic Photovoltaic Cells with Silver or Gold Electrodes. *Mol. Cryst. Liq. Cryst.* **2007**, *462*, 83–90.
2. Knoll, W. Interfaces and Thin Films as Seen by Bound Electromagnetic Waves. *Annu. Rev. Phys. Chem.* **1998**, *49*, 569–638.
3. Stenzel, O.; Stendal, A.; Roder, M.; Wilbrandt, S.; Drews, D.; Werninghaus, T.; von Borczyskowski, C.; Zahn, D. R. T. Localized Plasmon Excitation in Metal Nanoclusters as a Tool to Study Thickness-Dependent Optical Properties of Copper Phthalocyanine Ultrathin Films. *Nanotechnology* **1998**, *9*, 6–19.
4. Alieva, E. V.; Knippels, G. M. H.; Kuzik, L. A.; Mattei, G.; van der Meer, A. F. G.; Yakovlev, V. A. Sum-Frequency Generation Spectra of Thin Organic Films on Silver Enhanced Due to Surface Plasmon Excitation. *Phys. Status Solidi A* **1999**, *175*, 109–114.
5. Linss, V.; Stenzel, O.; Zahn, D. R. T. Correlation between Linear Optical Constants and Raman Enhancement in Phthalocyanine Thin Solid Films with Incorporated Silver Clusters. *J. Raman Spectrosc.* **1999**, *30*, 531–536.
6. Stenzel, O. Optical Properties of Noble Metal Clusters in Ultrathin Solid Films. *J. Cluster Sci.* **1999**, *10*, 169–193.
7. Hutter, E.; Fendler, J. H. Exploitation of Localized Surface Plasmon Resonance. *Adv. Mater.* **2004**, *16*, 1685–1706.
8. Ditlbacher, H.; Aussenegg, F. R.; Krenn, J. R.; Lamprecht, B.; Jakopic, G.; Leising, G. Organic Diodes as Monolithically Integrated Surface Plasmon Polariton Detectors. *Appl. Phys. Lett.* **2006**, *89*, 161101.
9. Kuila, B. K.; Garai, A.; Nandi, A. K. Synthesis, Optical, and Electrical Characterization of Organically Soluble Silver Nanoparticles and Their Poly(3-Hexylthiophene) Nanocomposites: Enhanced Luminescence Property in the Nanocomposite Thin Films. *Chem. Mater.* **2007**, *19*, 5443–5452.
10. Mapel, J. K.; Singh, M.; Baldo, M. A.; Celebi, K. Plasmonic Excitation of Organic Double Heterostructure Solar Cells. *Appl. Phys. Lett.* **2007**, *90*, 121102.
11. Uemura, T.; Furumoto, M.; Nakano, T.; Akai-Kasaya, M.; Salto, A.; Aono, M.; Kuwahara, Y. Local-Plasmon-Enhanced up-Conversion Fluorescence from Copper Phthalocyanine. *Chem. Phys. Lett.* **2007**, *448*, 232–236.
12. Sato, Y.; Yamagishi, K.; Yamashita, M. Multilayer Structure Photovoltaic Cells. *Opt. Rev.* **2005**, *12*, 324–327.
13. Schaadt, D. M.; Feng, B.; Yu, E. T. Enhanced Semiconductor Optical Absorption *via* Surface Plasmon Excitation in Metal Nanoparticles. *Appl. Phys. Lett.* **2005**, *86*, 063106.
14. Rand, B. P.; Peumans, P.; Forrest, S. R. Long-Range Absorption Enhancement in Organic Tandem Thin-Film Solar Cells Containing Silver Nanoclusters. *J. Appl. Phys.* **2004**, *96*, 7519–7526.
15. Westphalen, M.; Kreibig, U.; Rostalski, J.; Luth, H.; Meissner, D. Metal Cluster Enhanced Organic Solar Cells. *Sol. Energy Mater. Sol. Cells* **2000**, *61*, 97–105.
16. Tvingstedt, K.; Persson, N. K.; Inganas, O.; Rahachou, A.; Zozoulenko, I. V. Surface Plasmon Increase Absorption in Polymer Photovoltaic Cells. *Appl. Phys. Lett.* **2007**, *91*, 113514.
17. Morfa, A. J.; Rowlen, K. L.; Reilly, T. H.; Romero, M. J.; van de Lagemaat, J. Plasmon-Enhanced Solar Energy Conversion in Organic Bulk Heterojunction Photovoltaics. *Appl. Phys. Lett.* **2008**, *92*, 3.
18. Ebbesen, T. W.; Lezec, H. J.; Ghaemi, H. F.; Thio, T.; Wolff, P. A. Extraordinary Optical Transmission through Subwavelength Hole Arrays. *Nature* **1998**, *391*, 667–669.
19. Barnes, W. L.; Dereux, A.; Ebbesen, T. W. Surface Plasmon Subwavelength Optics. *Nature* **2003**, *424*, 824–830.
20. Genet, C.; Ebbesen, T. W. Light in Tiny Holes. *Nature* **2007**, *445*, 39–46.
21. Degiron, A.; Ebbesen, T. W. The Role of Localized Surface Plasmon Modes in the Enhanced Transmission of Periodic Subwavelength Apertures. *J. Opt. A* **2005**, *7*, S90–S96.
22. Degiron, A.; Ebbesen, T. W. Analysis of the Transmission Process through Single Apertures Surrounded by Periodic Corrugations. *Opt. Express* **2004**, *12*, 3694–3700.
23. Krishnan, A.; Thio, T.; Kima, T. J.; Lezec, H. J.; Ebbesen, T. W.; Wolff, P. A.; Pendry, J.; Martin-Moreno, L.; Garcia-Vidal, F. J. Evanescently Coupled Resonance in Surface Plasmon Enhanced Transmission. *Opt. Commun.* **2001**, *200*, 1–7.
24. Xiao, M. F.; Rakov, N. Enhanced Optical near-Field Transmission through Subwavelength Holes Randomly Distributed in a Thin Gold Film. *J. Phys.: Condens. Matter* **2003**, *15*, L133–L137.
25. Reilly, T. H.; van de Lagemaat, J.; Tenent, R. C.; Morfa, A. J.; Rowlen, K. L. Surface-Plasmon Enhanced Transparent Electrodes in Organic Photovoltaics. *Appl. Phys. Lett.* **2008**, *92*, 243304.
26. Rindzevicius, T.; Alaverdyan, Y.; Sepulveda, B.; Pakizeh, T.; Kall, M.; Hillenbrand, R.; Aizpurua, J.; de Abajo, F. J. G. Nanohole Plasmons in Optically Thin Gold Films. *J. Phys. Chem. C* **2007**, *111*, 1207–1212.
27. Alaverdyan, Y.; Sepulveda, B.; Eurenius, L.; Olsson, E.; Kall, M. Optical Antennas Based on Coupled Nanoholes in Thin Metal Films. *Nat. Phys.* **2007**, *3*, 884–889.
28. Altewischer, E.; van Exter, M. P.; Woerdman, J. P. Plasmon-Assisted Transmission of Entangled Photons. *Nature* **2002**, *418*, 304–306.
29. Maier, S. A. Plasmonics—Towards Subwavelength Optical Devices. *Curr. Nanosci.* **2005**, *1*, 17–23.
30. Maier, S. A.; Atwater, H. A. Plasmonics: Localization and Guiding of Electromagnetic Energy in Metal/Dielectric Structures. *J. Appl. Phys.* **2005**, *98*, 011101.
31. Ozbay, E. Plasmonics: Merging Photonics and Electronics at Nanoscale Dimensions. *Science* **2006**, *311*, 189–193.

32. Chang, S. H.; Gray, S. K.; Schatz, G. C. Surface Plasmon Generation and Light Transmission by Isolated Nanoholes and Arrays of Nanoholes in Thin Metal Films. *Opt. Express* **2005**, *13*, 3150–3165.
33. Ghaemi, H. F.; Thio, T.; Grupp, D. E.; Ebbesen, T. W.; Lezec, H. J. Surface Plasmons Enhance Optical Transmission through Subwavelength Holes. *Phys. Rev. B* **1998**, *58*, 6779–6782.
34. Thio, T.; Ghaemi, H. F.; Lezec, H. J.; Wolff, P. A.; Ebbesen, T. W. Surface-Plasmon-Enhanced Transmission through Hole Arrays in Cr Films. *J. Opt. Soc. Am. B* **1999**, *16*, 1743–1748.
35. Popov, E.; Neviere, M.; Enoch, S.; Reinisch, R. Theory of Light Transmission through Subwavelength Periodic Hole Arrays. *Phys. Rev. B* **2000**, *62*, 16100–16108.
36. Strelniker, Y. M. Theory of Optical Transmission through Elliptical Nanohole Arrays. *Phys. Rev. B* **2007**, *76*, 085409.
37. Martin-Moreno, L.; Garcia-Vidal, F. J.; Lezec, H. J.; Pellerin, K. M.; Thio, T.; Pendry, J. B.; Ebbesen, T. W. Theory of Extraordinary Optical Transmission through Subwavelength Hole Arrays. *Phys. Rev. Lett.* **2001**, *86*, 1114–1117.
38. Devaux, E.; Ebbesen, T. W.; Weeber, J. C.; Dereux, A. Launching and Decoupling Surface Plasmons *via* Micrograting. *Appl. Phys. Lett.* **2003**, *83*, 4936–4938.
39. Gao, H. W.; Henzie, J.; Odom, T. W. Direct Evidence for Surface Plasmon-Mediated Enhanced Light Transmission through Metallic Nanohole Arrays. *Nano Lett.* **2006**, *6*, 2104–2108.
40. Yin, L.; Vlasko-Vlasov, V. K.; Rydh, A.; Pearson, J.; Welp, U.; Chang, S. H.; Gray, S. K.; Schatz, G. C.; Brown, D. B.; Kimball, C. W. Surface Plasmons at Single Nanoholes in Au Films. *Appl. Phys. Lett.* **2004**, *85*, 467–469.
41. Murray, W. A.; Astilean, S.; Barnes, W. L. Transition from Localized Surface Plasmon Resonance to Extended Surface Plasmon−Polariton as Metallic Nanoparticles Merge to Form a Periodic Hole Array. *Phys. Rev. B* **2004**, *69*.
42. Haynes, C. L.; Van Duyne, R. P. Nanosphere Lithography: A Versatile Nanofabrication Tool for Studies of Size-Dependent Nanoparticle Optics. *J. Phys. Chem. B* **2001**, *105*, 5599–5611.
43. Hanarp, P.; Sutherland, D. S.; Gold, J.; Kasemo, B. Control of Nanoparticle Film Structure for Colloidal Lithography. *Colloids Surf., A* **2003**, *214*, 23–36.
44. Prikulis, J.; Hanarp, P.; Olofsson, L.; Sutherland, D.; Kall, M. Optical Spectroscopy of Nanometric Holes in Thin Gold Films. *Nano Lett.* **2004**, *4*, 1003–1007.
45. Bahns, J. T.; Yan, F. N.; Qiu, D. L.; Wang, R.; Chen, L. H. Hole-Enhanced Raman Scattering. *Appl. Spectrosc.* **2006**, *60*, 989–993.
46. Octavio, M; G, G.; Aponte, J. Conductivity and Noise Critical Exponents in Thin-Films near the Metal-Insulator Percolation Transition. *Phys. Rev. B* **1987**, *36*, 2461–2465.
47. Last, B. J.; Thouless, D. J. Percolation Theory and Electrical Conductivity. *Phys. Rev. Lett.* **1971**, *27*, 1719.
48. Doremus, R. H. Optical Properties of Small Clusters of Silver and Gold Atoms. *Langmuir* **2002**, *18*, 2436–2437.
49. Parsons, J.; Hendry, E.; Burrows, C. P.; Auguie, B.; Sambles, J. R.; Barnes, W. L. Localized Surface-Plasmon Resonances in Periodic Nondiffracting Metallic Nanoparticle and Nanohole Arrays. *Phys. Rev. B* **2009**, *79*, 073412.
50. Cole, J. R.; Halas, N. J. Optimized Plasmonic Nanoparticle Distributions for Solar Spectrum Harvesting. *Appl. Phys. Lett.* **2006**, *89*, 153120.